Received: 30 June 2022 | Accepted: 31 August 2022

DOI: 10.1111/1751-7915.14145

RESEARCH ARTICLE

microbial biotechnology Open Access

Salinomycin biosynthesis reversely regulates the β-oxidation pathway in *Streptomyces albus* by carrying a 3-hydroxyacyl-CoA dehydrogenase gene in its biosynthetic gene cluster

Jiaxiu Wei[1,2] | **Binbin Chen**[3] | **Jianxin Dong**[1,2] | **Xueyu Wang**[1,2] | **Yongquan Li**[1,2] | **Yingchun Liu**[4] | **Wenjun Guan**[1,2]

[1]The Fourth Affiliated Hospital, Zhejiang University School of Medicine, Hangzhou, China

[2]Zhejiang Provincial Key Laboratory for Microbial Biochemistry and Metabolic Engineering, Hangzhou, China

[3]ZJU-Hangzhou Global Scientific and Technological Innovation Center, Hangzhou, China

[4]Department of Chemistry, Zhejiang University, Hangzhou, China

Correspondence
Yingchun Liu, Department of Chemistry, Zhejiang University, Hangzhou, China.
Email: liuyingch@zju.edu.cn

Wenjun Guan, The Fourth Affiliated Hospital, Zhejiang University School of Medicine, Hangzhou, China.
Email: guanwj@zju.edu.cn

Funding information
the National Key R&D Program of China, Grant/Award Number: 2018YFA0903200 and 2019YFA0905400

Abstract

Streptomyces is well known for synthesis of many biologically active secondary metabolites, such as polyketides and non-ribosomal peptides. Understanding the coupling mechanisms of primary and secondary metabolism can help develop strategies to improve secondary metabolite production in *Streptomyces*. In this work, *Streptomyces albus* ZD11, an oil-preferring industrial *Streptomyces* strain, was proved to have a remarkable capability to generate abundant acyl-CoA precursors for salinomycin biosynthesis with the aid of its enhanced β-oxidation pathway. It was found that the salinomycin biosynthetic gene cluster contains a predicted 3-hydroxyacyl-CoA dehydrogenase (FadB3), which is the third enzyme of β-oxidation cycle. Deletion of *fadB3* significantly reduced the production of salinomycin. A variety of experimental evidences showed that FadB3 was mainly involved in the β-oxidation pathway rather than ethylmalonyl-CoA biosynthesis and played a very important role in regulating the rate of β-oxidation in *S. albus* ZD11. Our findings elucidate an interesting coupling mechanism by which a PKS biosynthetic gene cluster could regulate the β-oxidation pathway by carrying β-oxidation genes, enabling *Streptomyces* to efficiently synthesize target polyketides and economically utilize environmental nutrients.

INTRODUCTION

Streptomycetes have a great potential to produce many biologically active secondary metabolites (also known as natural products) (Berdy, 2005; Hwang et al., 2014). The production of secondary metabolites is highly dependent on the availability of biosynthetic precursors, most of which are products of primary metabolism (Olano et al., 2008; van Keulen et al., 2011). Changes in primary metabolism can result in knock-on effects on secondary metabolism. For example, although all *Streptomyces* strains harbour the similar primary metabolic pathways, their abilities to yield a same secondary metabolite are quite different (Kallifidas et al., 2018;

Jiaxiu Wei and Binbin Chen contributed equally to this work.

This is an open access article under the terms of the Creative Commons Attribution-NonCommercial-NoDerivs License, which permits use and distribution in any medium, provided the original work is properly cited, the use is non-commercial and no modifications or adaptations are made.
© 2022 The Authors. *Microbial Biotechnology* published by Society for Applied Microbiology and John Wiley & Sons Ltd.

Peng et al., 2018; Wang et al., 2013). In *Streptomyces*, to achieve efficient synthesis of a target secondary metabolite, it is necessary to understand intrinsic link between its biosynthetic pathway and primary metabolism, so as to optimize the related primary metabolic pathways and provide sufficient precursors for the biosynthesis of target secondary metabolite.

Polyketides are a large family of structurally diverse secondary metabolites exhibiting a vast array of biological and pharmacological activities such as antibacterial, antifungal, anticholesterol, antiparasitic, anticancer and immunosuppressive properties (Staunton & Weissman, 2001). Polyketide backbones are always assembled from starter and extender units derived from carboxylated acyl-coenzyme A (acyl-CoA) precursors, such as acetyl-CoA, malonyl-CoA (M-CoA), (2*S*)-methylmalonyl-CoA (MM-CoA), (2*S*)-ethylmalonyl-CoA (EM-CoA) and propionyl-CoA (P-CoA), via sequential Claisen-like condensation reactions catalysed by polyketide synthases (PKSs) (Chan et al., 2009). These precursors are mainly derived directly or indirectly from acetyl-CoA generated by glycolysis and fatty acid oxidation pathways.

In general, most *Streptomyces* strains preferentially utilize sugar as carbon source for cell growth and polyketide biosynthesis. This process mainly relies on the glycolytic pathway. Previous studies had found that oils, which are cheaper than other carbon sources, could also be employed as the main carbon source to produce polyketide antibiotics in several industrial *Streptomyces* strains (Efthimiou et al., 2008; Li et al., 2009; Wang, Liu, et al., 2017; Wang, Shan, et al., 2017). As the main component of oil, exogenous triglycerides (TAGs) can be hydrolysed into glycerol and free fatty acids (FFAs) via a series of secreted lipases (Alvarez & Steinbuchel, 2002). The majority of absorbed FFAs are finally broken down into acetyl-CoA through β-oxidation pathway, which always consists of five enzymatic steps (Figure S1) (Schulz, 1991). In *Escherichia coli*, FFAs are activated by thioesterification with CoA derivatives and subsequently undergo oxidation by an acyl-CoA synthetase (FadD, EC 6.2.1.3) (Black et al., 1992). After that, a four-step cycle begins with the generation of an unsaturation at the α-β position by acyl-CoA dehydrogenase (FadE, EC 1.3.8.7/8) (Cox et al., 2019; Fujita et al., 2007; Ghisla & Thorpe, 2004). The next step is carried out by enoyl-CoA hydratase (ECH, EC 4.2.1.17), which hydroxylates the carbon chain at β-position to produce β-hydroxyacyl-CoA. Its β-hydroxy group is subsequently oxidized by 3-hydroxyacyl-CoA dehydrogenase (3HCDH, EC1.1.1.35) to yield the β-keto group using NAD^+ as a cofactor (Cox et al., 2019; DiRusso, 1990; Elena Volodina1, 2014; Fujita et al., 2007). Interestingly, single 3-hydroxyacyl-CoA dehydrogenase can not only function as a dimer but also associate with the enoyl-CoA hydratase to form a complex to catalyse the reaction. Moreover, a 3HCDH domain and an ECH domain can form a multifunctional protein (FadB) to catalyse two-step reaction in β-oxidation cycle (Elena Volodina1, 2014; Menendez-Bravo et al., 2017; Yang et al., 1988). Previous studies showed that a purified 3-hydroxyacyl-CoA dehydrogenase (FadB2) in *Mycobacterium tuberculosis* catalysed not only the dehydration of (3S)-hydroxybutyryl-CoA to acetoacetyl-CoA at pH 10 but also the reverse reaction, converting acetoacetyl-CoA to (3S)-hydroxybutyryl-CoA in a lower pH range of 5.5–6.5 (Taylor et al., 2010). This type of protein often has conserved catalytic residues, such as Ser, His and Asn (Cox et al., 2019; Kim et al., 2014). The final step of β-oxidation cycle, catalysed by β-ketoacyl-CoA thiolase (FadA, EC 2.3.1.9/16), is the cleavage of β-ketoacyl-CoA to an acetyl-CoA and an acyl-CoA shortened by two carbon atoms (Yang et al., 1990). The shortened acyl-CoA re-enters the β-oxidation cycle, whereas acetyl-CoA enters the Krebs cycle and the fatty acid synthetic pathway or is transformed into the acyl-CoA precursors for polyketides biosynthesis (Chan et al., 2009).

Since the β-oxidation pathway is closely related to the supply of polyketide precursors, previous studies proposed several strategies to control the synthesis of downstream polyketides by manipulating the content of TAGs pool (Banchio & Gramajo, 1997; Hobbs et al., 1997; Wang et al., 2020). For example, the overexpression of fatty acyl-CoA synthetase in *Streptomyces coelicolor* could guide more acyl-CoAs into the β-oxidation cycle, resulting in more production of acetyl-CoA. The genomic analysis of *S. coelicolor* revealed many potential β-oxidation gene homologues, including three *fadAB* gene clusters (Menendez-Bravo et al., 2017). Deletion of these *fadAB* homologues could significantly impair the β-oxidation process and increase intracellular TAGs accumulation, which then reduced the production of acetyl-CoA.

Salinomycin produced by *Streptomyces albus* is a polyether antibiotic, which has been widely used as a food additive to prevent intestinal coccidiosis in poultry (Fuchs et al., 2010; Gumila et al., 1997; Kuo et al., 2012). Using a typical type I PKS (Figure S2A), the biosynthesis of salinomycin polyketide backbone requires one acetyl-CoA, five M-CoAs, six MM-CoAs and three EM-CoAs molecules as the biosynthetic precursors (Jiang et al., 2012). Most genes in the salinomycin biosynthetic gene cluster (BGC) are positively regulated by SlnR, which is a pathway-specific regulator (Zhu et al., 2017) (Figure S2B). *Streptomyces albus* ZD11 was derived from an industrial strain which preferred to use soybean oil as carbon source and could produce up to 8 g/L salinomycin in shake flasks (Zhu et al., 2017). Our previous study revealed the remarkable enrichment of genes related to TAGs metabolism in *S. albus* ZD11 according to comparative genomic analysis (Li et al., 2020). For example,

there are up to 101 predicted β-oxidation genes in *S. albus* ZD11, including 24 acyl-CoA synthetase genes, 39 acyl-CoA dehydrogenase genes, 17 enoyl-CoA hydratase genes, seven 3-hydroxyacyl-CoA dehydrogenase genes, 12 β-ketoacyl-CoA thiolase genes and also two genes encoding ECH-3HCDH multifunctional protein. In addition, the transcriptomic profiling showed that the expression levels of genes involved in fatty acid catabolic and synthetic pathways were significantly increased when using soybean oil as a sole carbon source in *S. albus* ZD11. It supports an inference that high efficiency of soybean oil utilization could provide abundant precursors for cell growth and high yield of salinomycin (Li et al., 2020). However, the way how these mentioned genes work together to make the β-oxidation pathway work efficiently is still unclear.

To clarify the relationship between the working efficiency of β-oxidation pathway and the high yield of salinomycin in *S. albus* ZD11, we focused on the 3-hydroxyacyl-CoA dehydrogenases in this study. By deletion of eight predicted 3-hydroxyacyl-CoA dehydrogenase genes in *S. albus* ZD11 (Table S1), it was confirmed that FadB1 (DUI70_0391), FadB2 (DUI70_0803) and FadB3 (DUI70_0275, also known as SlnP) were important for salinomycin production. Among them, *fadB3* locating inside the salinomycin BGC plays the most important role. The evidences from various experiments in this study suggest that the contribution of FadB3 to the high yield of salinomycin is mainly realized by enhancing fatty acid β-oxidation in *S. albus* ZD11. Our work showed for the first time that the *Streptomyces* strain could efficiently synthesize the polyketide with the help of additional β-oxidation genes carried by its PKS BGC.

EXPERIMENTAL PROCEDURES

Media and cultivation conditions

All experiments were performed with the strains and vectors listed in Table S2. Different vectors were propagated in *E. coli* cultured in Luria-Bertani (LB) medium at 37°C. To prepare spores, *S. albus* ZD11 and its derivative strains were cultivated on ISP4 agar plates (BD) for 10 days at 30°C. The *Streptomyces* strains were cultivated in tryptic soy broth (TSB) medium (3%) for 24 h growth at 30°C and 220 rpm to obtain high-quality genomic DNA for whole-genome sequencing and genotype confirmation. The industrial seed medium (soybean powder, 3%; glucose, 4%; yeast extract, 1%; $CaCO_3$, 0.1%) was used for seed cultivation for 29 h at 30°C and 220 rpm. Then, the seed cultures (10%) were inoculated into ionic medium (Li et al., 2020; Zhang et al., 2017) (NaCl, 0.5%; KCl, 0.5%; $[NH_4]_2SO_4$, 2%; $MgSO_4$, 0.02%; K_2HPO_4, 0.02%; $CaCl_2$, 0.01%; $CaCO_3$, 2%) with soybean oil (oil medium) or glucose (glucose medium) containing an equimolar amount of carbon (2.7 M) for 5-day growth at 32°C and 180 rpm. When appropriate, apramycin, spectinomycin, kanamycin or chloramphenicol was added to the medium at a final concentration of 50, 50, 50 or 25 μg/ml, respectively.

Construction of gene disruption mutants and analysis of the phenotypes

A previously constructed fosmid library was used to generate the SGD and MGD mutants of *S. albus* ZD11 (Zhu et al., 2017). The fosmids listed in Table S3 were used to construct the gene disruption mutants using the PCR-targeting system (Gust et al., 2003; Zhu et al., 2017). *fadB2* and *fadB9* were displaced by the spectinomycin and apramycin disruption cassette, respectively, as described previously (Wang, Liu, et al., 2017; Wang, Shan, et al., 2017). Other six *fadBs* were displaced by a 81 bp scar. The exconjugants were inoculated onto the ISP4 plates for two rounds of non-selective growth before selection by replica plating for sensitive colonies. In addition, the Δ*fadB2*Δ*fadB1* mutant was constructed by deleting the *fadB1* in the Δ*fadB2* mutant. *fadB3* and *fadB4* were knocked out in the Δ*fadB2*Δ*fadB1* mutant to construct the Δ*fadB2*Δ*fadB1*Δ*fadB3* mutant and the Δ*fadB2*Δ*fadB1*Δ*fadB4* mutant, respectively. All the mutants were confirmed by PCR, RT-qPCR and DNA-sequencing. Salinomycin yield was measured according to the method previously reported (Li et al., 2020). Five ml of fermentation broth was harvested at the end of fermentation (120 h) and then centrifuged for 10 min to remove the supernatant. After washing with equal volume methanol, the collected mycelia were dried in an oven at 80°C for 24 h to determine the dry weight.

RNA-seq analysis and quantitative real-time RT-PCR (RT-qPCR) assay

For total RNA extraction, *S. albus* ZD11 and its related mutants were grown in an ionic medium with soybean oil or glucose (0.45 M) as the sole carbon source. Three replicates of mycelia were collected at 36 h from the media and stored at −80°C until RNA extraction. Total RNA isolation and RNA-seq were performed according to a previous report (Wang, Liu, et al., 2017; Wang, Shan, et al., 2017). RT-qPCR was performed on a Mastercycler ep gradient S instrument (Eppendorf, Hamburg, Germany) using ChamQ STBR qPCR Master Mix (Vazyme, China) according to the manufacturer's guidelines. The expression level of target gene was internally normalized to housekeeping gene *hrdB (DUI70_1421)* and quantified by the $2^{-\triangle\triangle CT}$ method (Livak & Schmittgen, 2001). Technical triplicates of three biological repeats were performed per condition.

Phylogenetic analysis of 3-hydroxyacyl-CoA dehydrogenase orthologous

Firstly, domain compositions of nine 3-hydroxyacyl-CoA dehydrogenases were analysed based on Pfam database (https://pfam.xfam.org). All relative amino acids sequences of the proteins were obtained from GenBank in FASTA format. The alignment was then generated by CLUSTALW (Larkin et al., 2007) using manual adjustments. Neighbour-joining tree was constructed using MEGA11 (Tamura et al., 2021) and then landscaped by the iTOL (Interactive Tree of Life) online software (https://itol.embl.de/) (Letunic & Bork, 2016). 272 PKS BGCs in *Streptomyces* were collected from the MIBiG database (Kautsar et al., 2020). The amino sequences of predicted 3-hydroxyacyl-CoA dehydrogenase orthologous within the corresponding BGCs were downloaded to construct the phylogenetic tree according to the above method.

Protein expression and purification

The nucleotide sequence of *fadB3* was amplified from the genomic DNA of *S. albus* ZD11 and cloned into pET28a to generate the recombinant vector pETFadB3. *Escherichia coli* BL21(DE3)/pKJE7 was chosen for heterologous expression of FadB3. The overnight culture of recombinant *E. coli* BL21(DE3)/pKJE7 was inoculated into 1000 ml liquid LB medium with appropriate antibiotics and grown to an OD_{600} of 0.5–0.6 at 37°C. Then the strain was induced 16 h at 16°C by the addition of isopropyl-β-D-thiogalactopyranoside (IPTG) and L-arabinose to final concentration of 0.1 and 2.5 mM, respectively. The cells were harvested by centrifugation and resuspended in the lysis buffer (0.5 M NaCl, 10 mM imidazole, 1 mM DTT, 40 mM Tris–HCl, pH 7.6) and followed by cell disruption by sonication. After the recovery of supernatant by centrifugation, soluble FadB3 with double His_6 tag was purified using nickel-nitrilotriacetic acid (Ni-NTA) resin. The resulting resins were first washed with the washing buffer (300 mM NaCl, 150 mM imidazole, 1 mM DTT, 40 mM Tris–HCl, pH 7.6), and the target protein was then eluted with the elution buffer (300 mM NaCl, 500 mM imidazole, 1 mM DTT, 40 mM Tris–HCl, pH 7.6). The purified protein was confirmed by SDS-PAGE analysis. The enzyme was then dialyzed against 40 mM Tris–HCl buffer, pH 7.6, containing 150 mM NaCl and 10% glycerol. Purified FadB3 was concentrated and stored at −80°C for further use.

In vitro biochemical assays and product analysis by HPLC

Enzyme activity was measured by monitoring the conversion between acetoacetyl-CoA and (3S)-hydroxybutyryl-CoA using HPLC. When (3S)-hydroxybutyryl-CoA was used as the substrate, the reaction mixture (100 μl) contained 50 mM NAD^+, 25 μM FadB3, 25 μM (3S)-hydroxybutyryl-CoA, 10 mM $MgCl_2$ and 1 mM 1,4-dithiothreitol (DTT) in 40 mM Tris–HCl buffer (pH 7.6). When acetoacetyl-CoA was used as the substrate, the reaction mixture contained 50 mM NADH, 25 μM FadB3, 25 μM acetoacetyl-CoA, 10 mM $MgCl_2$ and 1 mM DTT in 40 mM Tris–HCl buffer (pH 7.6). All the above reaction mixtures were incubated at 30°C for different time and then quenched with two volumes of methanol. The supernatants were then subjected to HPLC analysis, which was carried out with an Agilent 1260 infinity system, using a ZORBAX Eclipse XDB-C18 column (4.6 × 150 mm, 5 μm). For the detection of two substrates after reaction, elution was performed at 0.8 $ml\,min^{-1}$ with a mobile-phase mixture consisting of a linear gradient of 50 mM ammonium acetate (pH 4.7) and methanol ([v/v]: 70:30, 0–25 min; 20:80, 25–30 min; 95:5, 30–38 min) (detection wavelength: 259 and 340 nm).

Computational methods of protein docking

The predicted protein structure of FadB3 was obtained from Robetta Server (Kim et al., 2004) (http://robetta.bakerlab.org), using an improved deep learning based on modelling method RoseTTAFold (Figure S10). The model of FadB3 has high conformation reliability based on the Ramachandran plot (Figure S11). Then the substrates were docked into FadB3 as the initial simulation structures by a flexible protein docking program AutoDock Vina (Trott & Olson, 2010). All simulations were performed with GROMACS 5.0 (Abraham et al., 2015) using an amber99sb force field. The force field parameters of the substrates (AA-CoA, HB-CoA, HCO-CoA and OCO-CoA) were constructed by Gaussian (Bahram & El-Shehawy, 2015) and ACPYPE (Vranken, 2012). The Berendsen thermostat and Parrinello-Rahman pressure coupling were applied to the system to maintain the constant temperature of 310 K and the constant pressure of 1.0 bar. Periodic boundary conditions were used in all simulations. The long-range electrostatic interaction with a cut-off distance of 1.2 nm was calculated by the particle mesh Ewald summation for the separation of the direct and reciprocal space. The cut-off of non-bonded van der Waals interaction was set at a distance of 1.2 nm. Bond lengths were constrained by the linear constraint solver algorithm (Hess et al., 1997). A docked substrate–protein binding configuration was first placed in a $10 \times 10 \times 10\ nm^3$ box. Then water molecules were added as the solvents. Sodium and chloride ions were also included in the system to maintain electrical neutrality. Simulations were carried out with a time step of 2 fs. The system was equilibrated by 50,000 steps of energy minimization, as well as 1 ns MD simulation in the NVT

ensemble and 2 ns in the NPT ensemble. Stable configurations were obtained after 50 ns (or 100 ns in some systems) of MD balance. Configurations in this study were visualized by VMD (Humphrey et al., 1996) and Pymol (DeLano, 2002).

Heterologous biosynthesis of daunorubicin (DNR) in *S. albus* ZD11

The 40.64 kb daunorubicin BGC consisting of 37 genes was directly cloned from the genomic DNA of *S. coeruleorubidus* into a linear p15A vector using RecET direct cloning and got the vector p15A-DNR. After inserting the cassette for conjugation and PhiC31 site-specific recombination (*oriT-phiC31*) into the p15A using Redαβ recombination, the *E. coli–Streptomyces* shuttle vector pDNR1 was obtained (Wang et al., 2016). The vector pDNR2 was obtained by replacing chloramphenicol resistance gene with apramycin resistance gene (*aac[3]IV*) in pDNR1. Then the promoter (172 bp) of *dnrI* in pDNR2 was replaced by a strong constitutive promoter *kasOp** (Wang et al., 2013) to generate the vector pDNR3. The shunt pathway genes, *dnrH*, *dnrX* and *dnrU* (Hutchinson, 1997; Shrestha et al., 2019), were deleted from pDNR3 to generate the vector pDNR4. The S2 mutant (Δ*sal*Δ*fadB3*) was constructed based on the S1 mutant (Δ*sal*), which was constructed in our previous study (Dong et al., 2021). pDNR4 was respectively transferred into the S1 and S2 mutant to construct the S3 (Δ*sal*Δ*fadB3*::pDNR4) and S4 (Δ*sal*::pDNR4) mutants.

About 100 μl of fermentation broth was extracted using 900 μl of methanol for 12 h and centrifuged at 12,000 rpm for 10 min. The supernatant was filtered through 0.22-μm filters and the yield of daunorubicin was detected by HPLC, using a ZORBAX Eclipse XDB-C18 column on the Shimadzu LC-20AT system. The biomass was determined by dry weight measurement mentioned above. For the detection of DNR, elution was performed at 1 ml min^{-1} with a mobile-phase mixture consisting of a linear gradient of 10 mM ammonium acetate in water (phase A) and acetonitrile (phase B). Elution was performed as follows: a linear gradient from 20% to 50% solvent B from 0 to 15 min, a linear gradient from 50% to 90% solvent B from 15 to 18 min and 90% solvent B from 18 to 22 min (detection wavelength: 254 nm).

RESULTS

Multiple analysis revealed the importance of 3-hydroxyacyl-CoA dehydrogenases in the β-oxidation pathway of *S. albus* ZD11

To investigate the distinctiveness of β-oxidation pathway in *S. albus* ZD11, we carried out a comparative genomic analysis between *S. albus* ZD11 and three commonly used *Streptomyces* strains (*S. coelicolor* A3[2], *S. albidoflavus* J1074 and *S. lividans* TK24), which can utilize both glucose and oil as the carbon sources (Kuo et al., 2012). According to the COG (Clusters of Orthologous Groups) database and the KEGG (Kyoto Encyclopedia of Genes and Genomes) database (Huerta-Cepas et al., 2019; Kanehisa & Goto, 2000), it was found that not only the total number of β-oxidation genes but also the amount of genes involved in every single step of β-oxidation pathway were significantly higher in *S. albus* ZD11 than those in the other three strains (Figure 1A,B). Next, the result of transcriptomic analysis indicates that the genes belonging to the β-oxidation pathway exhibited higher expression levels when *S. albus* ZD11 was cultured in the soybean oil medium compared to the glucose medium (Figure 1C). Interestingly, although the total number of 3-hydroxyacyl-CoA dehydrogenase genes (abbreviated to *fadBs*) is minimal among the five reaction steps of the β-oxidation pathway in *S. albus* ZD11, the sum of FPKM values (Fragments Per Kilobase per Million) of these genes is the highest when the strain was cultured in the soybean oil medium. Among them, the FPKM value of *fadB3* was the highest, and that of *fadB7* was the lowest and less than the lower limit of gene expression level (FPKM value <10) defined in this study. The transcriptional levels of five of the nine *fadBs* were significantly upregulated in the soybean oil medium (Figures 1D and S3). Surprisingly, *fadB3* was found to locate inside the biosynthetic gene cluster of salinomycin and was positively regulated by the pathway-specific regulator SlnR (Figure S2B). According to our previous study, the transcriptional level of *fadB3* was decreased over 90% in the *slnR* deletion mutant and was significantly increased in the *slnR* overexpression mutant compared to that in the WT strain (Jiang et al., 2012).

According to the analysis of conserved domains base on Pfam database (Mistry et al., 2021), the nine predicted 3-hydroxyacyl-CoA dehydrogenases were divided into four classes (Figure 1E). In the first class, FadB1 and FadB2 consist of an *N*-terminal crotonase-like family/enoyl-CoA hydratase domain (pfam00378), a central 3-hydroxyacyl-CoA dehydrogenase-NAD binding domain (3HCDH_N, pfam02737) and C-terminal 3-hydroxyacyl-CoA dehydrogenase domain (3HCDH, pfam00725). These two proteins showed high identities to the known fatty acid oxidative multifunctional enzyme SCO6732 (84.49%) and SCO6026 (88.59%) from *S. coelicolor* (Menendez-Bravo et al., 2017), implying FadB1 and FadB2 are the multifunctional proteins with both ECH and 3HCDH activities. In the second class, FadB3 and FadB9 have two 3HCDH_N domains and two 3HCDH domains. The domain composition of FadB5 was similar to the second class, which had a 3HCDH_RFF (pfam18321, a 3HCDH_N

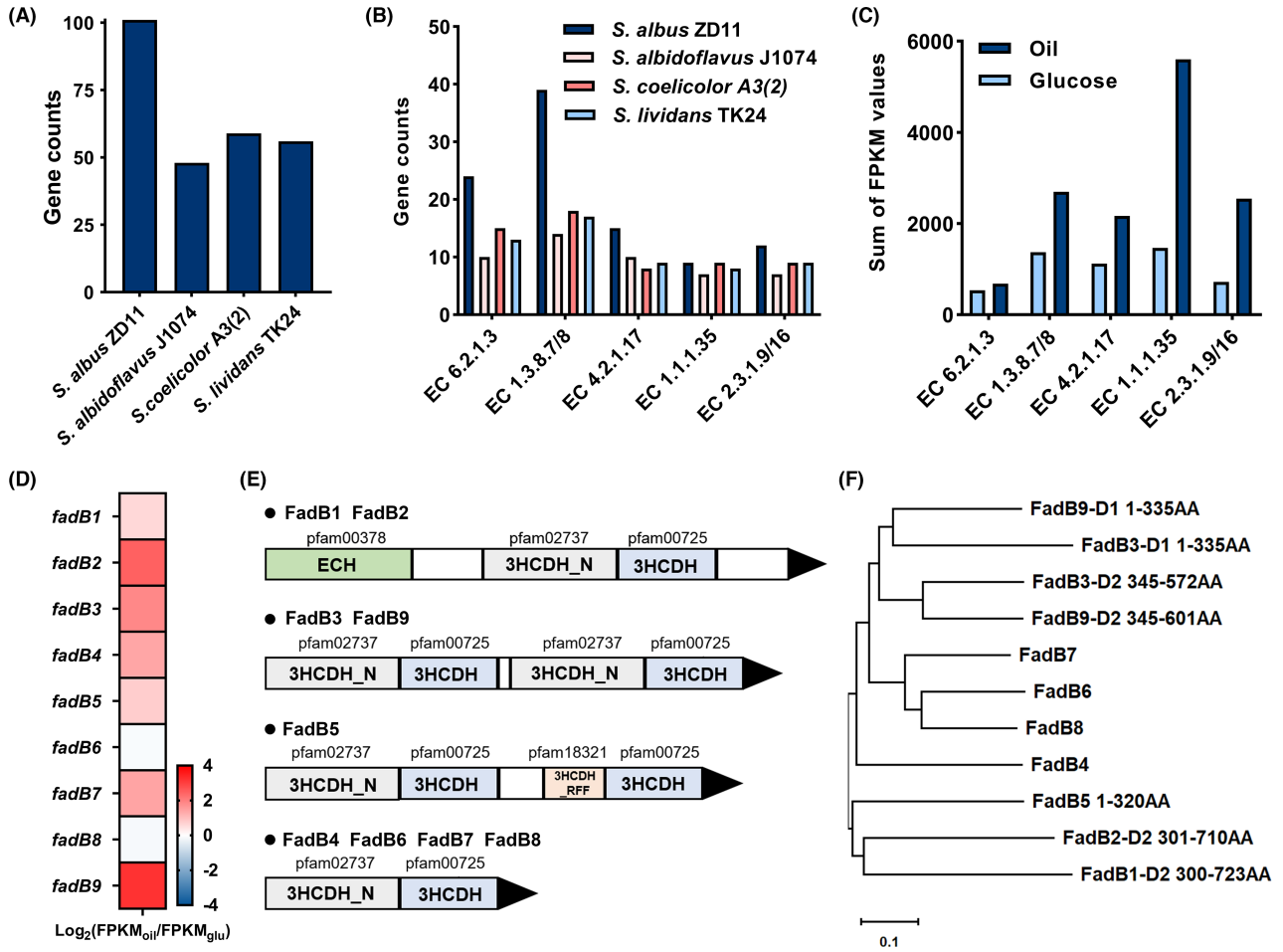

FIGURE 1 Multiple analysis of the genes predicted to involve in the β-oxidation pathway of *S. albus* ZD11. (A) Quantities of predicted β-oxidation genes in *S. albus* ZD11, *S. albidoflavus* J1074, *S. coelicolor* A3(2) *and S. lividans* TK24. (B) Quantities of genes involved in each step of β-oxidation pathway. (C) The sum of FPKM values of genes in each step of β-oxidation pathway when the *S. albus* ZD11 WT strain was cultured in the medium using soybean oil or glucose as sole carbon source. (D) The fold changes in expression levels of nine 3-hydroxyacyl-CoA dehydrogenase genes in the oil medium relative to those in the glucose medium. RNA fold change is the normalized $\log_2$ ratio of FPKM values ($FPKM_{oil}/FPKM_{glucose}$). (E) Analysis of the domain composition of nine 3-hydroxyacyl-CoA dehydrogenases. (F) Phylogenetic tree of the 3HCDH_N-3HCDH units from nine 3-hydroxyacyl-CoA dehydrogenases. Phylogenetic tree was reconstructed using the neighbour-joining algorithm implemented in MEGA11. Scale bar represents 0.1 estimated sequence divergence. D1 and D2, respectively, represent the *N*-terminal and C-terminal 3HCDH_N-3HCDH units located in the corresponding 3-hydroxyacyl-CoA dehydrogenases.

missing the catalytic residues and an NAD [H] binding cleft) instead of 3HCDH_N at the N-terminal part. The last class includes FadB4, FadB6, FadB7 and FadB8, which consist of only one 3HCDH_N domain and one 3HCDH domain. According to the previous reports (Cox et al., 2019; Menendez-Bravo et al., 2017; Taylor et al., 2010), the members in the last class of 3-hydroxyacyl-CoA dehydrogenase perhaps function by assembling into a dimer. In addition, phylogenetic analysis showed that all 3HCDH_N-3HCDH units from the four classes of 3-hydroxyacyl-CoA dehydrogenase could be classified into two clades (Figure 1F). Clade I contains eight 3HCDH_N-3HCDH units located in FadB3, FadB4, FadB6, FadB7, FadB8 and FadB9, respectively. Clades II contains three 3HCDH_N-3HCDH units belonging to FadB1, FadB2 and FadB5. It suggests that the function of members in each group might be more similar.

FadB3 presents a core status among the 3-hydroxyacyl-CoA dehydrogenases in *S. albus* ZD11

To investigate the role of predicted 3-hydroxyacyl-CoA dehydrogenases in *S. albus* ZD11, we tried to knock out each 3-hydroxyacyl-CoA dehydrogenase gene by PCR targeting (Zhu et al., 2017) and constructed a series of single-gene deletion (SGD) mutants, except *fadB8* because of its low transcriptional level under the existing fermentation conditions. Compared to the WT strain, the salinomycin yields of eight SGD mutants

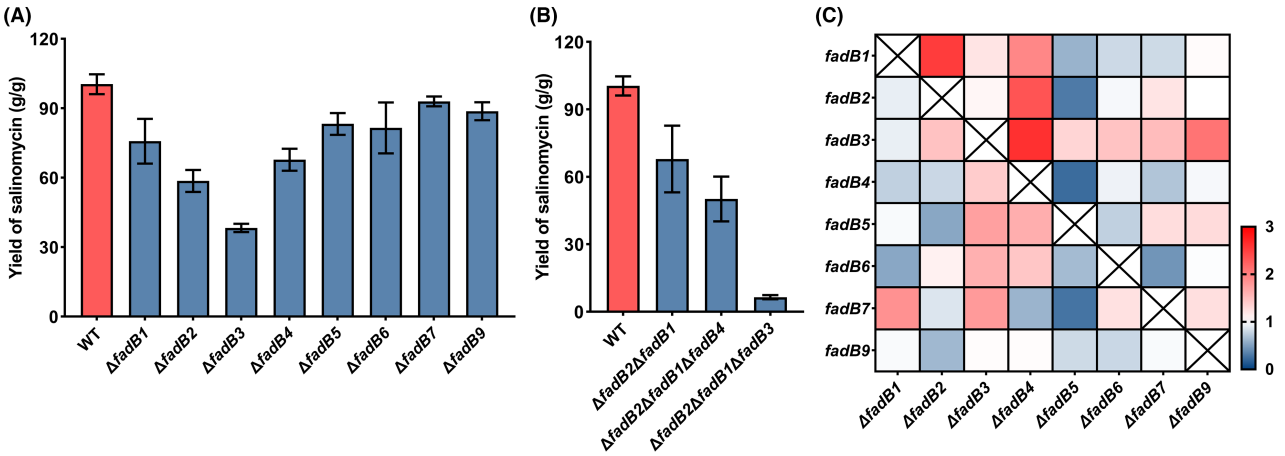

FIGURE 2 Deletion of the *fadBs* decreased the salinomycin production of *S. albus* ZD11. (A) The relative salinomycin yields of the SGD mutants. (B) The relative salinomycin yields of the MGD mutants. Error bars indicate the SD for samples tested in triplicate. (C) Expression level analysis of the remaining 3-hydroxyacyl-CoA dehydrogenase genes in each SGD mutant as compared to the WT strain. *hrdB* transcription was monitored and used as the internal control. Each fold change was calculated by RT-qPCR using the $2^{-\triangle\triangle CT}$ method. The data are presented as the average of three parallel samples.

were all decreased. The Δ*fadB1*, Δ*fadB2*, Δ*fadB3* and Δ*fadB4* mutants showed more significant reduction in salinomycin production than the other SGD mutants. Among them, the Δ*fadB3* mutant exhibited the least yield of salinomycin (Figure 2A). Moreover, the biomass of each SGD mutant was almost the same as that of the WT strain, indicating that knockout of each 3-hydroxyacyl-CoA dehydrogenase gene alone did not affect cell growth (Figure S4A).

To figure out how these 3-hydroxyacyl-CoA dehydrogenases work together in *S. albus* ZD11, the expression levels of remaining *fadBs* in each SGD mutant were measured. As shown in Figure 2C, the expression level of each remaining *fadB* gene in the Δ*fadB3* mutant was more or less upregulated. At the same time, the expression level of *fadB3* was upregulated in almost all other SGD mutants except the Δ*fadB1* mutants. This indicates that *fadB3* could be upregulated to recover the loss of other *fadB* genes and vice versa, suggesting its central role among the *fadBs* in *S. albus* ZD11.

Then several multi-gene deletion (MGD) mutants were constructed in order to further analyse the effect of FadB1, FadB2, FadB3 or FadB4 on salinomycin production. As shown in Figure 2B, the salinomycin yield of the Δ*fadB2*Δ*fadB1* mutant was less than that of the Δ*fadB1* mutant or the Δ*fadB2* mutant. Compared to the Δ*fadB2*Δ*fadB1* mutant, the Δ*fadB2*Δ*fadB1*Δ*fadB3* mutant showed a remarkable drawdown in salinomycin yield, while the Δ*fadB2*Δ*fadB1*Δ*fadB4* mutant exhibited a relative less reduction. These results further determined the critical role of FadB3. In addition, these MGD mutants presented no obvious reduction in biomass compared to the WT strain, implying that the remaining *fadBs* in the mutants are still able to keep the β-oxidation pathways working properly for primary metabolism in *S. albus* ZD11 (Figure S4B).

The 3-hydroxyacyl-CoA dehydrogenase orthologous located inside the PKS BGCs show no inevitable connection with the biosynthesis of EM-CoA

Since *fadB3* locates within the salinomycin BGC, previous studies suggested that FadB3 might participate in the biosynthesis of EM-CoA precursor (Jiang et al., 2012; Lu et al., 2016), but there was no experimental evidence to confirm this. To investigate the association between the β-oxidation genes within PKS BGCs and the biosynthesis of corresponding polyketides, we collected 272 PKS BGCs from the MIBiG database (Kautsar et al., 2020) (Appendix S1). It was found that more than half of these BGCs do not contain the predicted β-oxidation genes and 10 of such BGCs are considered to use EM-CoA as the biosynthetic precursor. On the contrary, there are 126 PKS BGCs containing the predicted β-oxidation genes, and 30 of them harbour at least one 3-hydroxyacyl-CoA dehydrogenase gene. 11 of the 30 BGCs are supposed to use EM-CoA as the biosynthetic precursor, implying that the 3-hydroxyacyl-CoA dehydrogenase genes located within the BGCs, at least, might be not just related to the biosynthesis of EM-CoA (Figure 3A). Except the 3-hydroxyacyl-CoA dehydrogenase genes, the genes predicted to encode acyl-CoA synthetase, acyl-CoA dehydrogenase or enoyl-CoA hydratase are also found in these PKS BGCs (Figure 3B, Appendix S1). And the acyl-CoA synthetase genes account for the highest proportion. Phylogenetic analysis showed that the 3HCDH_N-3HCDH units from the thirty-one 3-hydroxyacyl-CoA dehydrogenase orthologous could be classified into three clades (Figure 3C). Six 3-hydroxyacyl-CoA dehydrogenases (including FadB3

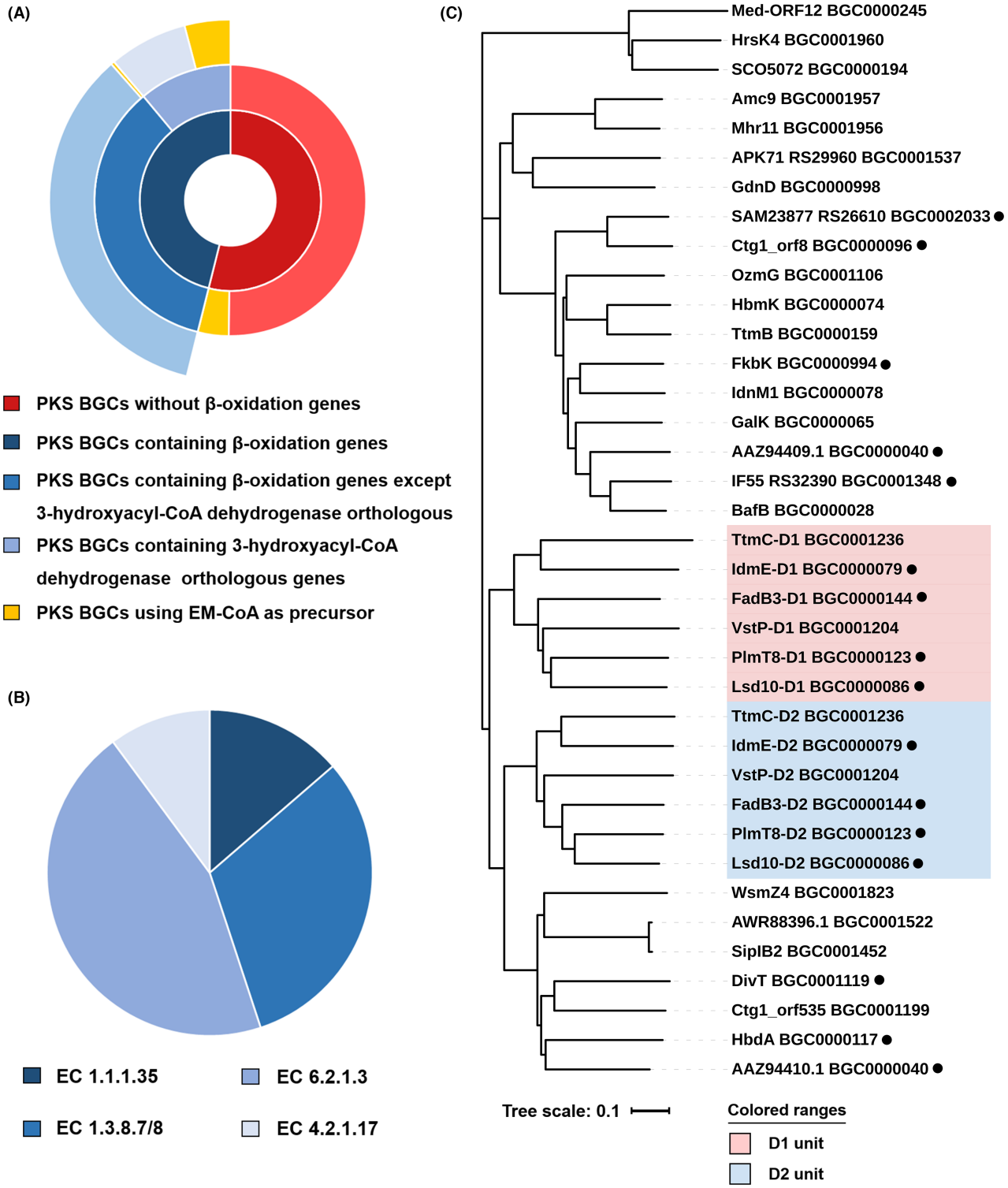

FIGURE 3 Relationship between the PKS BGCs and the β-oxidation genes within these BGCs. (A) Distribution of the PKS BGCs collected from the MIBiG database. (B) Distribution of the PKS BGCs containing β-oxidation genes. (C) Phylogenetic tree of 3HCDH_N-3HCDH units from the 3-hydroxyacyl-CoA dehydrogenases located in the 30 PKS BGCs. Phylogenetic tree was reconstructed using the neighbour-joining algorithm implemented in MEGA 11. Scale bar represents 0.1 estimated sequence divergence. D1 unit and D2 unit represent the N-terminal and C-terminal 3HCDH_N-3HCDH units located in the corresponding 3-hydroxyacyl-CoA dehydrogenases. Black dots represent the 3-hydroxyacyl-CoA dehydrogenase from the PKS BGCs using EM-CoA as a biosynthetic precursor.

in *S. albus* ZD11) containing two 3HCDH_N-3HCDH units all belong to clade III, indicating their closer evolutionary relationships. These results demonstrate that the 3-hydroxyacyl-CoA dehydrogenase orthologous found in the PKS BGCs are not necessarily associated with EM-CoA biosynthesis.

FadB3 prefers to catalyse the conversion of 3-hydroxyacyl-CoA to the 3-ketoyl acid to enhance the β-oxidation pathway in *S. albus* ZD11

3-Hydroxyacyl-CoA dehydrogenase is the penultimate enzyme in β-oxidation cycle and reversibly catalyses the conversion of 3-hydroxyacyl-CoA to 3-ketoacyl-CoA. To evaluate its catalytic activity, *fadB3* was cloned from *S. albus* ZD11 and heterologously expressed in *E. coli* BL21 (DE3) to get the purified protein (Figure 4A). According to the previous reports, the activity of 3-hydroxyacyl-CoA dehydrogenase was usually measured by NAD^+/NADH-dependent dehydrogenase reaction using acetoacetyl-CoA or (3S)-hydroxybutyryl-CoA as the short-chain acyl-CoA substrate (Elena Volodina1, 2014; Taylor et al., 2010). As shown in Figure 4B, under the condition of pH 7.6 which is within the range of physiological pH in *Streptomyces* cell, FadB3 could catalyse the conversion of (3S)-hydroxybutyryl-CoA to acetoacetyl-CoA much better than the reverse reaction. After 90 minutes of catalysis, more than two-thirds of (3S)-hydroxybutyryl-CoA was transformed to acetoacetyl-CoA, but only few acetoacetyl-CoA was converted to (3S)-hydroxybutyryl-CoA. Since one of the pathways involved in EM-CoA biosynthesis is started with converting acetoacetyl-CoA to (3S)-hydroxybutyryl-CoA (Figure S1), our result gave the evidence that FadB3 prefers to participate in the β-oxidation pathway rather than the synthesis of EM-CoA.

To validate the catalytic results above and figure out the possibility of long-chain acyl-CoAs catalysed by FadB3, we thus turned to computational approaches to gain mechanistic insight into the enzymatic properties of FadB3. As the docking results of short-chain acyl-CoAs showed, AA-CoA and HB-CoA were docking with FadB3-D1 (N-terminal 3HCDH_N-3HCDH unit of FadB3) and FadB3-D2 (C-terminal 3HCDH_N-3HCDH unit of FadB3), respectively. Two representative binding conformations were selected due to their stability for further analysis (Figure S5A,B). RMSF (Root Mean Square Fluctuation) and RMSD (Root Mean Square Deviation) showed that FadB3 could combine with short-chain acyl-CoAs appropriately and stably (Figures S6 and 5A,B). Analysis of the conformation structures revealed that the short-chain acyl-CoAs were probably positioned near the residues Thr18, Thr229, His130 and Lys264 in FadB3-D1 (Figures 6A,B and S7A,C). And Asn480, His430, Asn433 and Pro515 could stabilize the short-chains probably in FadB3-D2 (Figures 6C,D and S7B,D). As shown in Figure S8, sequence alignment showed that His130 in FadB3-D1 and His430 in FadB3-D2 were conserved compared to His143 in FadB2 from *M. tuberculosis* and His140 in PaaH1 from *Ralstonia eutropha*, which were reported as the conserved catalytic residues (Cox et al., 2019; Kim et al., 2014). Therefore, there is a great possibility that short-chain acyl-CoAs could be catalysed in FadB3-D1 and FadB3-D2 according to the results of MD simulations, which can be mutually verified with above experimental results (Figure 4B). Then the substrates were extended to long-chain acyl-CoAs based on the validity of MD simulations. Because the main fatty acids of soybean oil is oleic acid, (3S)-hydroxy-9Z-octadecenoyl-CoA and (9Z)-3-oxooctadecenoyl-CoA were chosen as the long-chain substrates of FadB3. Representative binding conformations between long-chain acyl-CoAs and FadB3 were also selected due to their stability for further mechanistic study. Our results showed that the interaction energy between long-chain acyl-CoAs

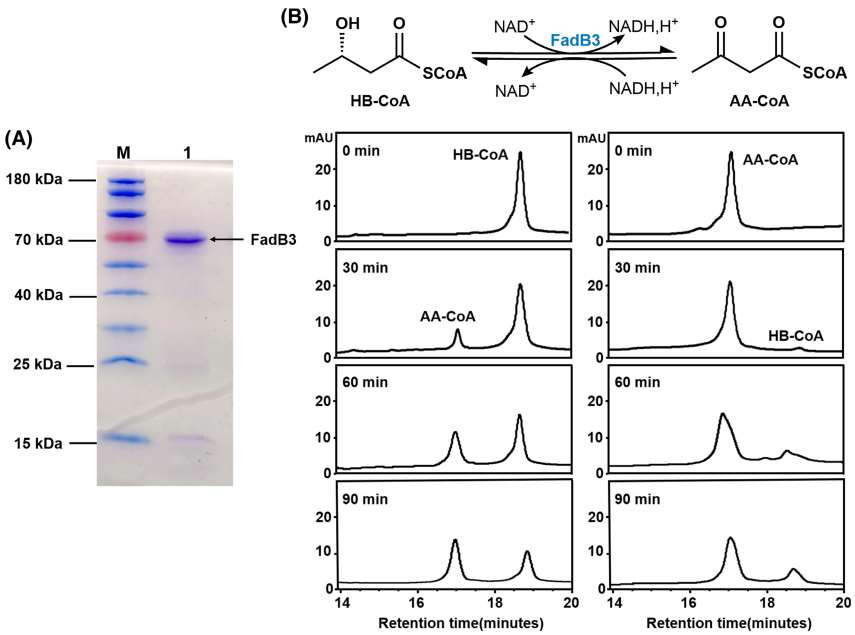

FIGURE 4 Evaluation of the catalytic activity of FadB3. (A) SDS-PAGE gel image of the purified FadB3 (64.9 kDa). Lane 1: purified FadB3 with N-terminal and C-terminal His6 tag. Lane M: protein marker. Adobe Photoshop (PS) CC 2018 was used for image editing. (B) FadB3 catalysed the NAD^+/NADH-dependent reaction between (3S)-hydroxybutyryl-CoA (HB-CoA) and acetoacetyl-CoA (AA-CoA). The contents of acetoacetyl-CoA and (3S)-hydroxybutyryl-CoA were determined by HPLC analysis (high performance liquid chromatography).

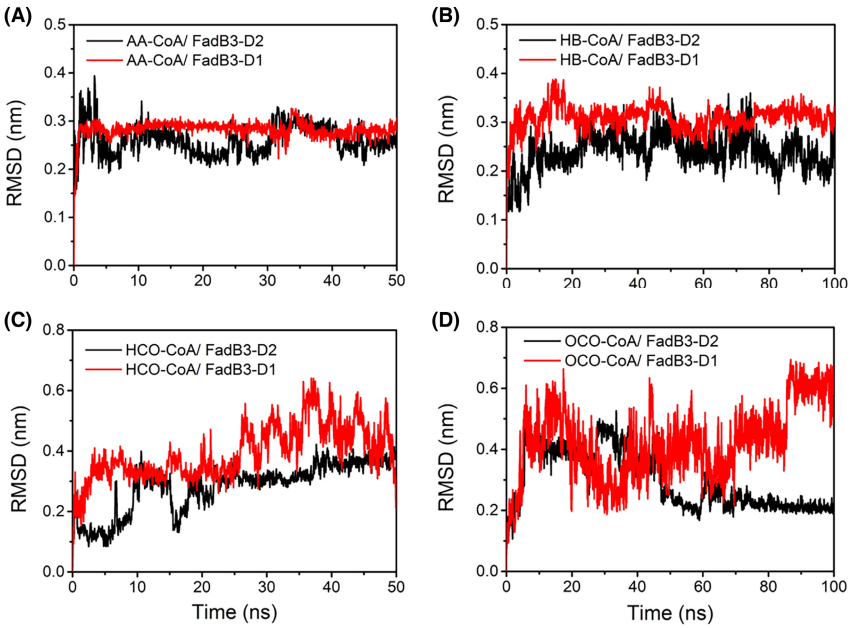

FIGURE 5 RMSD of acyl-CoAs located in different domains of FadB3. (A) acetoacetyl-CoA (AA-CoA). (B) (3S)-hydroxybutyryl-CoA (HB-CoA). (C) (3S)-hydroxy-9Z-octadecenoyl-CoA (HCO-CoA). (D) (9Z)-3-oxooctadecenoyl-CoA (OCO-CoA).

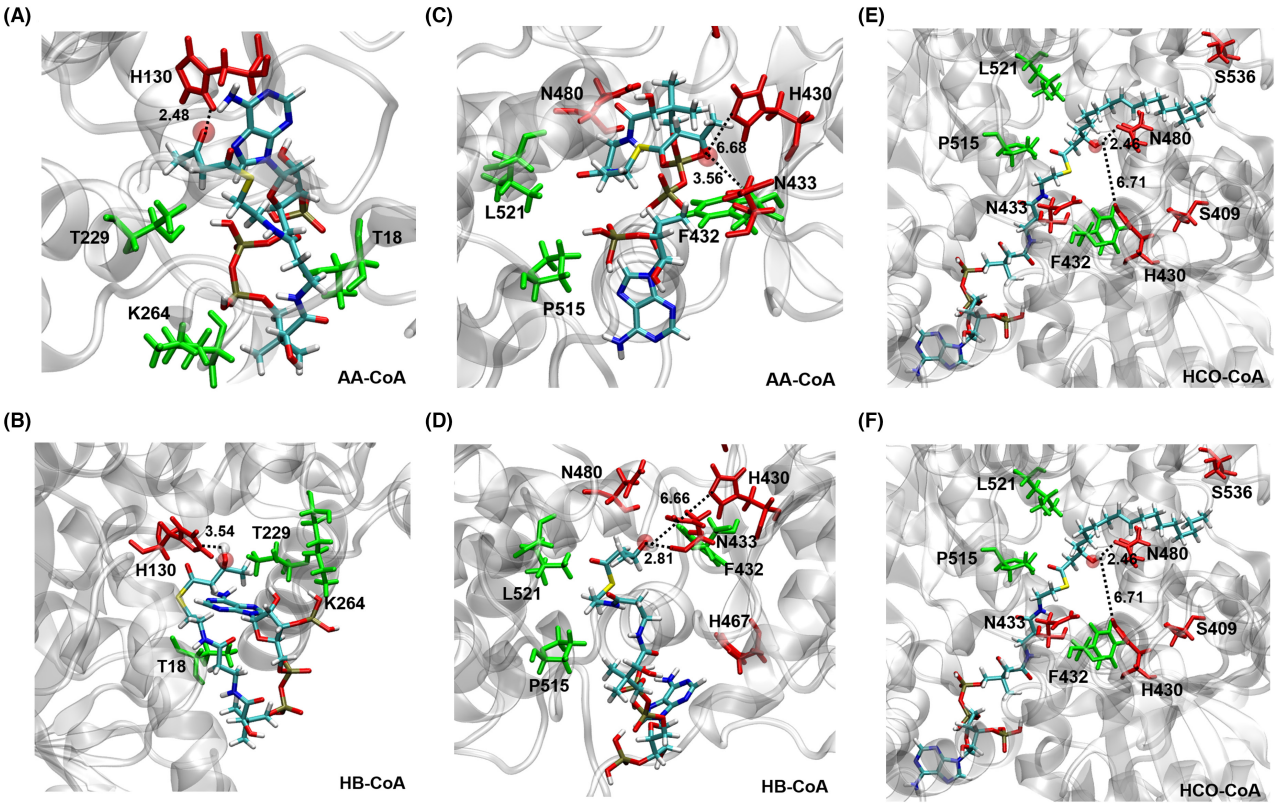

FIGURE 6 Binding configurations of substrates and FadB3. (A) FadB3-D1 combines with AA-CoA; (B) FadB3-D1 combines with HB-CoA; (C) FadB3-D2 combines with AA-CoA; (D) FadB3-D2 combines with HB-CoA; (E) FadB3-D2 combines with HCO-CoA; (F) FadB3-D2 combines with OCO-CoA.

and FadB3 was mainly van der Waals and with no obvious difference comparing with short-chain acyl-CoAs (Figure S9). However, FadB3-D2 could combine with long-chain acyl-CoAs more stable than FadB3-D1 according to the less fluctuation of RMSD in FadB3-D2 (Figure 5C,D), which might be due to the flexible long carbon chains. Furthermore, the possible catalytic residue Asn480 was observed in the conformation of long-chain acyl-CoAs with FadB3-D2 (Figures 6E,F and S7E,F). However, any possible catalytic residues could not be found at the binding site when long-chain acyl-CoAs were combined with the

FadB3-D1. In conclusion, these results indicate that FadB3-D2 can not only bind short-chain acyl-CoAs but also long-chains acyl-CoAs. Based on the above analysis, FadB3 can bind short-chain and long-chain acyl-CoAs with different preferences, suggesting its ability to act as a key 3-hydroxyacyl-CoA dehydrogenase to catalyse oxidation of both short-chain and long-chain acyl-CoAs in the β-oxidation process, but the oxidation of short-chain acyl-CoAs may occur more easily.

Heterologous biosynthesis of daunorubicin (DNR) further confirmed the key role of FadB3 played in the β-oxidation pathway of *S. albus* ZD11

Since FadB3 could also catalyse the conversion from acetoacetyl-CoA to (3S)-hydroxybutyryl-CoA with lower efficiency in vitro, whether the significant reduction in salinomycin yield of Δ*fadB3* mutant is more influenced by β-oxidation or EM-CoA biosynthesis is still uncertain. To explain that, a daunorubicin (DNR) BGC was cloned from *Streptomyces coeruleorubidus* and heterogeneously expressed in *S. albus* ZD11. DNR is synthesized by a type II PKS. This PKS assembles 10 precursors consisting of one P-CoA starter unit and nine M-CoA extender units into the anthracyclinone skeleton of DNR (Blumauerova et al., 1977; Malla et al., 2010) (Figure 7A). Most of the genes in the DNR BGC are regulated by a pathway-specific regulator DnrI (Tang et al., 1996). The S2 mutant (Δ*sal*Δ*fadB3*) based on a S1 (Δ*sal*) mutant that cannot produce salinomycin anymore (Figure S2C) (Dong et al., 2021) was constructed in this study. The vector (pDNR4) carrying an engineered DNR BGC was integrated into the chromosome of S2 or S1 mutants, respectively. As shown in Figure 7B,C, the S4 (Δ*sal*Δ*fadB3*::pDNR4) mutant produced 47% of DNR less than the S3 (Δ*sal*::pDNR4) mutant when using

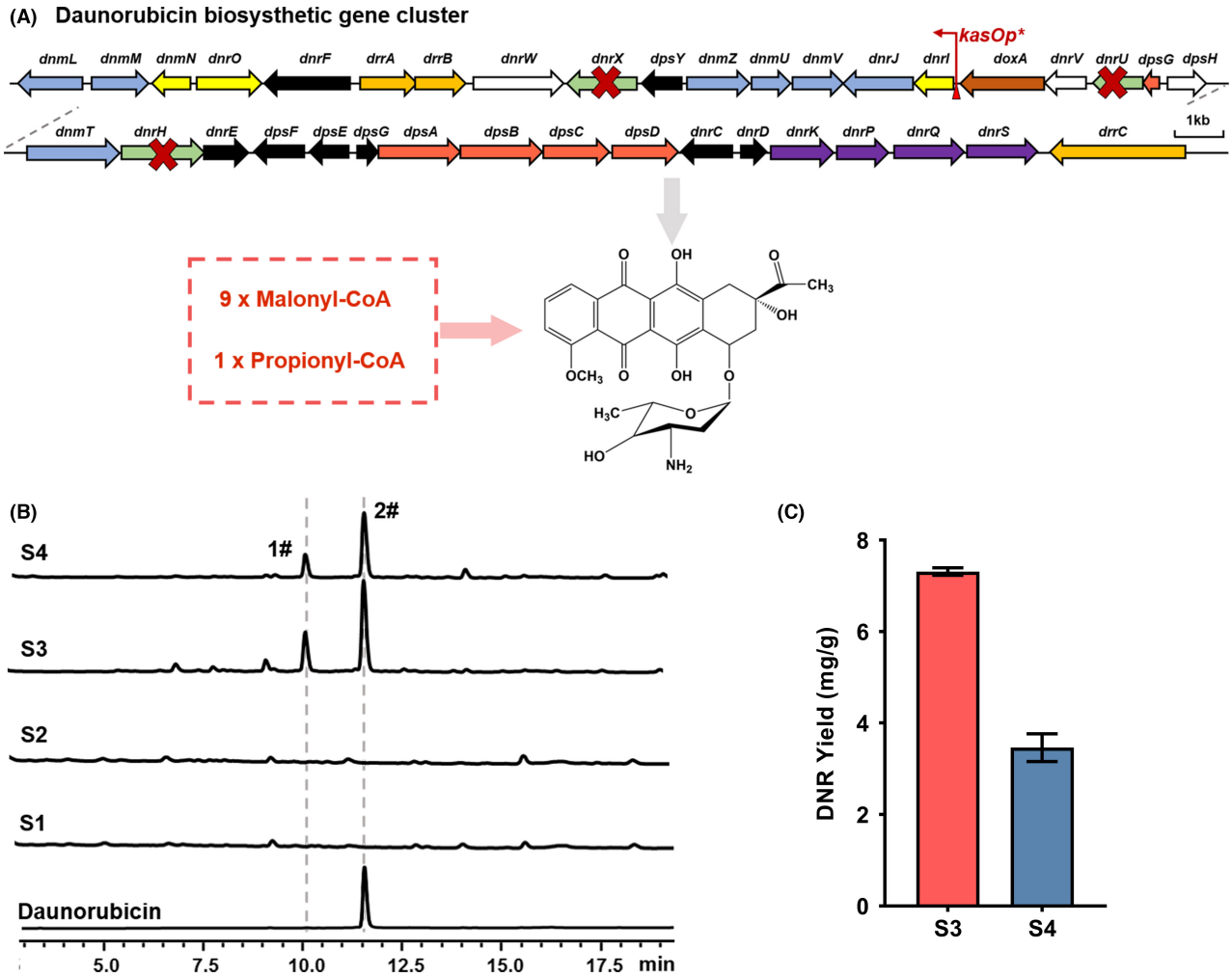

FIGURE 7 Heterologous biosynthesis of daunorubicin in *S. albus* ZD11. (A) Engineering the promoter of *dnrI* (a pathway-specific regulator gene) and blocking the shunt pathways in DNR BGC. (B) HPLC analysis of the yield of daunorubicin in the S1 (Δ*sal*), S2 (Δ*sal*Δ*fadB3*), S3 (Δ*sal*::pDNR4) or S4 (Δ*sal*Δ*fadB3*::pDNR4) mutant. 1# and 2# peaks represent 13-dihydrodaunorubicin and DNR, respectively. (C) The production of daunorubicin in the S3 and S4 mutants. Error bars indicate the *SD* for samples tested in triplicate.

soybean oil as sole carbon source. We suggest that the β-oxidation pathway lacking *fadB3* decreases the generation of acetyl-CoA, which in turn reduces M-CoA production in S4 mutant and leads to a reduction in DNR production compared to the S3 mutant. Since biosynthesis of DNR does not use EM-CoA as a precursor, this result further confirmed the key role of FadB3 played in the β-oxidation pathway of *S. albus* ZD11.

DISCUSSION

In *Streptomyces*, understanding the coupling mechanisms of primary and secondary metabolism could enable the development of strategies to improve the production of target secondary metabolites. Genomic and transcriptomic analysis indicates that *S. albus* ZD11 has a remarkable capability to generate abundant acyl-CoA precursors for salinomycin biosynthesis with the help of its enhanced β-oxidation pathway. In this work, 3-hydroxyacyl-CoA dehydrogenase that is the penultimate enzyme in the β-oxidation cycle was carefully studied. We found that a 3-hydroxyacyl-CoA dehydrogenase gene (*fadB3*) carried by the salinomycin BGC played a very important role in adjusting the rate of β-oxidation in *S. albus* ZD11. Deletion of *fadB3* significantly reduced the production of salinomycin. The evidences from in vitro enzymatic activity detection, protein–substrate docking and heterologous expression of DNR BGC all proved that FadB3 mainly involved in the β-oxidation pathway rather than EM-CoA biosynthesis.

Since *fadB3* is positively regulated by the pathway-specific regulator SlnR, it should start to function only after the biosynthesis of salinomycin is initiated. As mentioned earlier, the amount of 3-hydroxyacyl-CoA dehydrogenase genes is minimal among the five steps of β-oxidation pathway in *S. albus* ZD11, suggesting 3-hydroxyacyl-CoA dehydrogenase might be the rate-limiting step. Thus, we proposed a mechanism of how salinomycin biosynthesis regulates the rate of fatty acid oxidation in *S. albus* ZD11. As shown in Figure 8, when salinomycin synthesis was initiated, *fadB3* was then highly expressed, which relieved the rate limitation caused by the lack of 3-hydroxyl-CoA dehydrogenases. This would result in more generation of acetyl-CoAs, most of which were subsequently converted to various acyl-CoA precursors for salinomycin biosynthesis (Figure S1). On the contrary, when the strain did not synthesize salinomycin, *fadB3* would not be activated to express, and the remaining 3-hydroxyacyl-CoA dehydrogenases would enable the β-oxidation pathway to operate at a relatively low rate to economically utilize nutrients in the environment.

Here, we report a very interesting mechanism by which a secondary metabolic pathway reversely regulates the primary metabolic processes. The PKS BGCs could regulate the β-oxidation pathway by carrying the

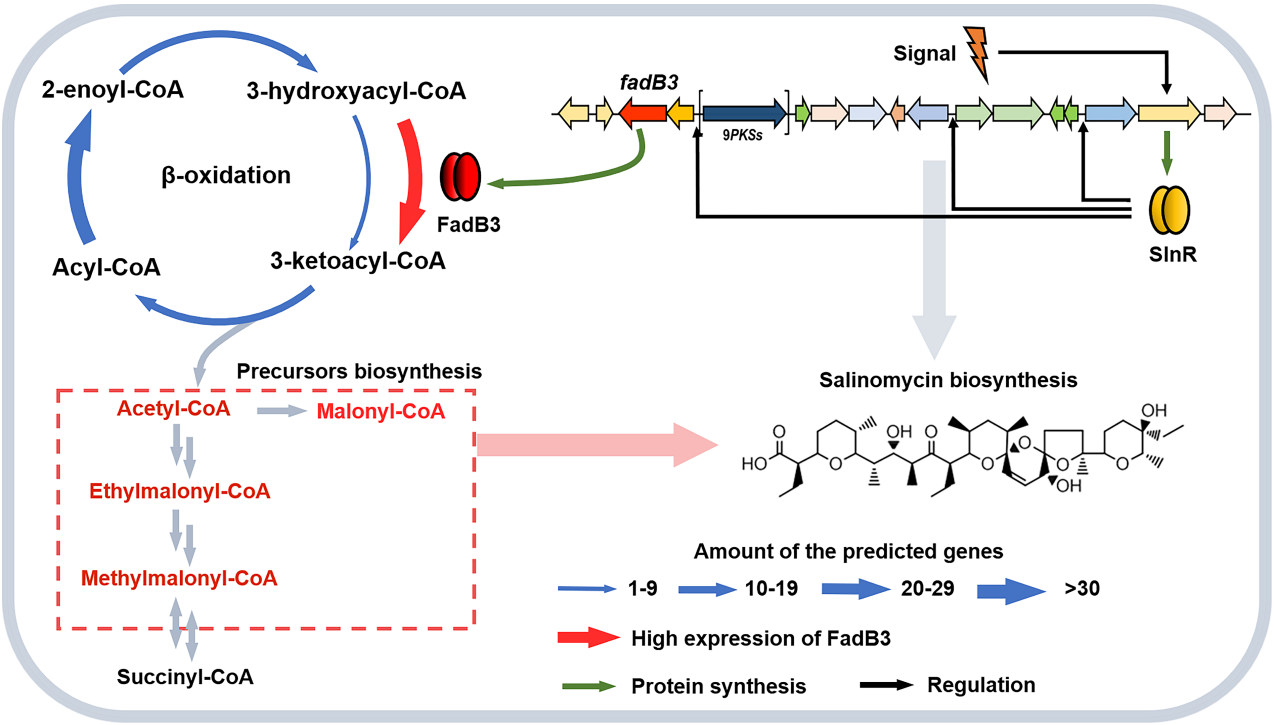

FIGURE 8 Schematic diagram of the proposed regulatory mechanism of the salinomycin biosynthesis on the β-oxidation pathway in *S. albus* ZD11.

β-oxidation genes, enabling *Streptomyces* strains to efficiently synthesize polyketides. By analysing more PKS BGCs, we found such mechanism might be widespread. Nearly 50% of the investigated PKS BGCs contain predicted β-oxidation genes, including the genes encoding acyl-CoA synthetase, acyl-CoA dehydrogenase, 3-hydroxyacyl-CoA dehydrogenase or enoyl-CoA hydratase, suggesting that they may play the similar roles like FadB3.

Although we used computational approaches to confirm that FadB3 could bind short-chain and long-chain acyl-CoAs with different preferences, it is still unclear how FadB3 catalyses the acyl-CoAs with different chain length. Besides, the protein–substrate docking predicted several key catalytic sites in FadB3, and it has not been experimentally verified, which is worth to study in our future work. It is also worth noticing that the existing methods for protein function prediction cannot accurately distinguish 3-hydroxyacyl-CoA dehydrogenase and 3-hydroxybutyryl-CoA dehydrogenase. Thus, functions of the other predicted 3-hydroxyacyl-CoA dehydrogenase in *S. albus* ZD11 still remain uncertain and need further study in the future.

AUTHOR CONTRIBUTIONS

J. X. Wei and **W. J. Guan** designed the study. **J. X. Wei** wrote the manuscript. **J. X. Wei, J. X. Dong and X. Y. Wang** performed the wet-lab experiments. **B. B. Chen** and **Y. C. Liu** designed and performed the protein-ligand docking experiments. **J. X. Wei** and **B. B. Chen** analysed the data. **W. J. Guan** and **Y. C. Liu** revised the manuscript. All authors read and approved the final manuscript.

ACKNOWLEDGMENTS

This work was financially supported by the National Key R&D Program of China (2019YFA0905400, 2018YFA0903200).

CONFLICT OF INTEREST

The authors declare no competing interests.

DATA AVAILABILITY STATEMENT

Genomic sequences of *S. albus* ZD11 (CP033071.1), *S. albidoflavus* J1074 (CP004370.1), *S. coelicolor* A3(2) (AL645882.2) and *S. lividans* TK24 (NZ_CP009124.1) were obtained from GenBank in GenBank format. The sequence reads obtained by RNA-seq were obtained from in the SRA database under accession numbers SAMN12251778, SAMN12251779, SAMN12251780 and SAMN12251781, which were described in our previous work (Li et al., 2020).

ORCID

Yongquan Li https://orcid.org/0000-0001-6013-4068
Wenjun Guan https://orcid.org/0000-0002-6485-8941

REFERENCES

Abraham, M.J., Murtola, T., Schulz, R., Páll, S., Smith, J.C., Hess, B. et al. (2015) GROMACS: high performance molecular simulations through multi-level parallelism from laptops to supercomputers. *SoftwareX*, 1-2, 19–25.

Alvarez, H.M. & Steinbuchel, A. (2002) Triacylglycerols in prokaryotic microorganisms. *Applied Microbiology and Biotechnology*, 60, 367–376.

Bahram, A. & El-Shehawy, S.A. (2015) Study of the convergence of the increments of gaussian process. *Applied Mathematics*, 06, 933–939.

Banchio, C. & Gramajo, H.C. (1997) Medium- and long-chain fatty acid uptake and utilization by *Streptomyces coelicolor* A3(2): first characterization of a gram-positive bacterial system. *Microbiol-Sgm*, 143, 2439–2447.

Berdy, J. (2005) Bioactive microbial metabolites. *Journal of Antibiotics (Tokyo)*, 58, 1–26.

Hess, B., Bekker, H., Berendsen, H.J.C. & Fraaije, J.G.E.M. (1997) LINCS: a Linear Constraint Solver for Molecular Simulations. *Journal of Computational Chemistry*, 18, 1463–1472.

Black, P.N., Dirusso, C.C., Metzger, A.K. & Heimert, T.L. (1992) Cloning, sequencing, and expression of the *fadD* gene of *Escherichia coli* encoding acyl coenzyme A synthetase. *The Journal of Biological Chemistry*, 267, 25513–25520.

Blumauerova, M., Mateju, J., Stajner, K. & Vanek, Z. (1977) Studies on the production of daunomycinone-derived glycosides and related metabolites in *Streptomyces coeruleorubidus* and *Streptomyces peucetius*. *Folia Microbiologia (Praha)*, 22, 275–285.

Chan, Y.A., Podevels, A.M., Kevany, B.M. & Thomas, M.G. (2009) Biosynthesis of polyketide synthase extender units. *Natural Product Reports*, 26, 90–114.

Cox, J.A.G., Taylor, R.C., Brown, A.K., Attoe, S., Besra, G.S. & Futterer, K. (2019) Crystal structure of *Mycobacterium tuberculosis* FadB2 implicated in mycobacterial β-oxidation. *Acta Crystallographica Section D: Structural Biology*, 75, 101–108.

DeLano, W.L. (2002) PyMOL: An Open-Source Molecular Graphics Tool. *CCP4 Newsl Protein Crystallography*, 40, 82–92.

DiRusso, C.C. (1990) Primary sequence of the *Escherichia coli fadBA* operon, encoding the fatty acid-oxidizing multienzyme complex, indicates a high degree of homology to eucaryotic enzymes. *Journal of Bacteriology*, 172, 6459–6468.

Dong, J., Wei, J., Li, H., Zhao, S. & Guan, W. (2021) An efficient markerless deletion system suitable for the industrial strains of *Streptomyces*. *Journal of Microbiology and Biotechnology*, 31, 1722–1731.

Efthimiou, G., Thumser, A.E. & Avignone-Rossa, C.A. (2008) A novel finding that *Streptomyces clavuligerus* can produce the antibiotic clavulanic acid using olive oil as a sole carbon source. *Journal of Applied Microbiology*, 105, 2058–2064.

Elena Volodina1, A.S. (2014) (S)-3-hydroxyacyl-CoA dehydrogenase/enoyl-CoA hydratase (FadB') from fatty acid degradation operon of *Ralstonia eutropha* H16. *AMB Express*, 4, 69.

Fuchs, D., Daniel, V., Sadeghi, M., Opelz, G. & Naujokat, C. (2010) Salinomycin overcomes ABC transporter-mediated multidrug and apoptosis resistance in human leukemia stem cell-like KG-1a cells. *Biochemical and Biophysical Research Communications*, 394, 1098–1104.

Fujita, Y., Matsuoka, H. & Hirooka, K. (2007) Regulation of fatty acid metabolism in bacteria. *Molecular Microbiology*, 66, 829–839.

Ghisla, S. & Thorpe, C. (2004) Acyl-CoA dehydrogenases. A mechanistic overview. *European Journal of Biochemistry*, 271, 494–508.

Gumila, C., Ancelin, M.L., Delort, A.M., Jeminet, G. & Vial, H.J. (1997) Characterization of the potent in vitro and in vivo antimalarial activities of ionophore compounds. *Antimicrobial Agents and Chemotherapy*, 41, 523–529.

Gust, B., Challis, G.L., Fowler, K., Kieser, T. & Chater, K.F. (2003) PCR-targeted *Streptomyces* gene replacement replacement identifies a protein domain needed for biosynthesis of the sesquiterpene soil odor geosmin. *Proceedings of the National Academy of Sciences of the United States of America*, 100, 1541–1546.

Hobbs, D.H., Kim, H.J., Chater, K.F. & Hills, M.J. (1997) Mutants of lipid synthesis in *Streptomyces coelicolor*. *Biochemical Society Transactions*, 25, S674.

Huerta-Cepas, J., Szklarczyk, D., Heller, D., Hernandez-Plaza, A., Forslund, S.K., Cook, H. et al. (2019) eggNOG 5.0: a hierarchical, functionally and phylogenetically annotated orthology resource based on 5090 organisms and 2502 viruses. *Nucleic Acids Research*, 47, D309–D314.

Humphrey, W., Dalke, A. & Schulten, K. (1996) VMD: Visual molecular dynamics. *Journal of Molecular Graphics*, 14, 33–38.

Hutchinson, C.R. (1997) Biosynthetic studies of daunorubicin and tetracenomycin C. *Chemical Reviews*, 97, 2525–2536.

Hwang, K.S., Kim, H.U., Charusanti, P., Palsson, B.O. & Lee, S.Y. (2014) Systems biology and biotechnology of *Streptomyces* species for the production of secondary metabolites. *Biotechnology Advances*, 32, 255–268.

Jiang, C., Wang, H., Kang, Q., Liu, J. & Bai, L. (2012) Cloning and characterization of the polyether salinomycin biosynthesis gene cluster of *Streptomyces albus* XM211. *Applied and Environmental Microbiology*, 78, 994–1003.

Kallifidas, D., Jiang, G., Ding, Y. & Luesch, H. (2018) Rational engineering of *Streptomyces albus* J1074 for the overexpression of secondary metabolite gene clusters. *Microbial Cell Factories*, 17, 25.

Kanehisa, M. & Goto, S. (2000) KEGG: Kyoto Encyclopedia of Genes and Genomes. *Nucleic Acids Research*, 28, 27–30.

Kautsar, S.A., Blin, K., Shaw, S., Navarro-Munoz, J.C., Terlouw, B.R., van der Hooft, J.J.J. et al. (2020) MIBiG 2.0: a repository for biosynthetic gene clusters of known function. *Nucleic Acids Research*, 48, D454–D458.

Kim, D.E., Chivian, D. & Baker, D. (2004) Protein structure prediction and analysis using the Robetta server. *Nucleic Acids Research*, 32, W526–W531.

Kim, J., Chang, J.H. & Kim, K.J. (2014) Crystal structure and biochemical properties of the (S)-3-hydroxybutyryl-CoA dehydrogenase PaaH1 from *Ralstonia eutropha*. *Biochemical and Biophysical Research Communications*, 448, 163–168.

Kuo, S.Z., Blair, K.J., Rahimy, E., Kiang, A., Abhold, E., Fan, J.B. et al. (2012) Salinomycin induces cell death and differentiation in head and neck squamous cell carcinoma stem cells despite activation of epithelial-mesenchymal transition and Akt. *BMC Cancer*, 12, 556.

Larkin, M.A., Blackshields, G., Brown, N.P., Chenna, R., McGettigan, P.A., McWilliam, H. et al. (2007) Clustal W and Clustal X version 2.0. *Bioinformatics*, 23, 2947–2948.

Letunic, I. & Bork, P. (2016) Interactive tree of life (iTOL) v3: an online tool for the display and annotation of phylogenetic and other trees. *Nucleic Acids Research*, 44, W242–W245.

Li, C., Hazzard, C., Florova, G. & Reynolds, K.A. (2009) High titer production of tetracenomycins by heterologous expression of the pathway in a *Streptomyces cinnamonensis* industrial monensin producer strain. *Metabolic Engineering*, 11, 319–327.

Li, H., Wei, J., Dong, J., Li, Y., Li, Y., Chen, Y. et al. (2020) Enhanced triacylglycerol metabolism contributes to efficient oil utilization and high-level production of salinomycin in *Streptomyces albus* ZD11. *Applied and Environmental Microbiology*, 86, e00763-20.

Livak, K.J. & Schmittgen, T.D. (2001) Analysis of relative gene expression data using real-time quantitative PCR and the 2(-Delta Delta C[T]) Method. *Methods*, 25, 402–408.

Lu, C., Zhang, X., Jiang, M. & Bai, L. (2016) Enhanced salinomycin production by adjusting the supply of polyketide extender units in *Streptomyces albus*. *Metabolic Engineering*, 35, 129–137.

Malla, S., Niraula, N.P., Singh, B., Liou, K. & Sohng, J.K. (2010) Limitations in doxorubicin production from *Streptomyces peucetius*. *Microbiological Research*, 165, 427–435.

Menendez-Bravo, S., Paganini, J., Avignone-Rossa, C., Gramajo, H. & Arabolaza, A. (2017) Identification of FadAB complexes involved in fatty acid beta-oxidation in *Streptomyces coelicolor* and construction of a triacylglycerol overproducing strain. *Frontiers in Microbiology*, 8, 1428.

Mistry, J., Chuguransky, S., Williams, L., Qureshi, M., Salazar, G.A., Sonnhammer, E.L.L. et al. (2021) Pfam: the protein families database in 2021. *Nucleic Acids Research*, 49, D412–D419.

Olano, C., Lombo, F., Mendez, C. & Salas, J.A. (2008) Improving production of bioactive secondary metabolites in actinomycetes by metabolic engineering. *Metabolic Engineering*, 10, 281–292.

Peng, Q., Gao, G., Lu, J., Long, Q., Chen, X., Zhang, F. et al. (2018) Engineered *Streptomyces lividans* strains for optimal identification and expression of cryptic biosynthetic gene clusters. *Frontiers in Microbiology*, 9, 3042.

Schulz, H. (1991) Beta oxidation of fatty acids. *Biochimica et Biophysica Acta*, 1081, 109–120.

Shrestha, B., Pokhrel, A.R., Darsandhari, S., Parajuli, P., Sohng, J.K. & Pandey, R.P. (2019) Engineering *Streptomyces peucetius* for doxorubicin and daunorubicin biosynthesis. *Environmental Chemistry for a Sustainable World*, 26, 191–209.

Staunton, J. & Weissman, K.J. (2001) Polyketide biosynthesis: a millennium review. *Natural Product Reports*, 18, 380–416.

Tamura, K., Stecher, G. & Kumar, S. (2021) MEGA11: Molecular Evolutionary Genetics Analysis Version 11. *Molecular Biology and Evolution*, 38, 3022–3027.

Tang, L., Grimm, A., Zhang, Y.X. & Hutchinson, C.R. (1996) Purification and characterization of the DNA-binding protein DnrI, a transcriptional factor of daunorubicin biosynthesis in *Streptomyces peucetius*. *Molecular Microbiology*, 22, 801–813.

Taylor, R.C., Brown, A.K., Singh, A., Bhatt, A. & Besra, G.S. (2010) Characterization of a beta-hydroxybutyryl-CoA dehydrogenase from *Mycobacterium tuberculosis*. *Microbiology (Reading)*, 156, 1975–1982.

Trott, O. & Olson, A.J. (2010) AutoDock Vina: improving the speed and accuracy of docking with a new scoring function, efficient optimization, and multithreading. *Journal of Computational Chemistry*, 31, 455–461.

van Keulen, G., Siebring, J. & Dijkhuizen, L. (2011) Central carbon metabolic pathways in *Streptomyces*. In: Dyson, P. (Ed.) *Streptomyces*. Norfolk: Caister Academic Press, pp. 105–124.

Vranken, A.W.S.d.S.W.F. (2012) ACPYPE - AnteChamber PYthon Parser interfacE. *BMC Research Notes*, 5, 367.

Wang, W., Li, X., Wang, J., Xiang, S., Feng, X. & Yang, K. (2013) An engineered strong promoter for streptomycetes. *Applied and Environmental Microbiology*, 79, 4484–4492.

Wang, H., Li, Z., Jia, R., Hou, Y., Yin, J., Bian, X. et al. (2016) RecET direct cloning and Redαβ recombineering of biosynthetic gene clusters, large operons or single genes for heterologous expression. *Nature Protocols*, 11, 1175–1190.

Wang, J., Liu, H., Huang, D., Jin, L., Wang, C. & Wen, J. (2017) Comparative proteomic and metabolomic analysis of *Streptomyces tsukubaensis* reveals the metabolic mechanism of FK506 overproduction by feeding soybean oil. *Applied Microbiology and Biotechnology*, 101, 2447–2465.

Wang, T.J., Shan, Y.M., Li, H., Dou, W.W., Jiang, X.H., Mao, X.M. et al. (2017) Multiple transporters are involved in natamycin efflux in *Streptomyces chattanoogensis* L10. *Molecular Microbiology*, 103, 713–728.

Wang, W., Li, S., Li, Z., Zhang, J., Fan, K., Tan, G. et al. (2020) Harnessing the intracellular triacylglycerols for titer improvement

of polyketides in *Streptomyces*. *Nature Biotechnology*, 38, 76–83.

Yang, S.Y., Li, J.M., He, X.Y., Cosloy, S.D. & Schulz, H. (1988) Evidence that the *fadB* gene of the *fadAB* operon of *Escherichia coli* encodes 3-hydroxyacyl-coenzyme-A (CoA) epimerase, delta-3-cis-delta 2-trans-enoyl-CoA isomerase, and enoyl-CoA hydratase in addition to 3-hydroxyacyl-CoA dehydrogenase. *Journal of Bacteriology*, 170, 2543–2548.

Yang, S.Y., Yang, X.Y., Healy-Louie, G., Schulz, H. & Elzinga, M. (1990) Nucleotide sequence of the *fadA* gene. Primary structure of 3-ketoacyl-coenzyme A thiolase from *Escherichia coli* and the structural organization of the *fadAB* operon. *Journal of Biological Chemistry*, 265, 10424–10429.

Zhang, X., Lu, C. & Bai, L. (2017) Conversion of the high-yield salinomycin producer *Streptomyces albus* BK3-25 into a surrogate host for polyketide production. *Science China Life Sciences*, 60, 1000–1009.

Zhu, Z., Li, H., Yu, P., Guo, Y., Luo, S., Chen, Z. et al. (2017) SlnR is a positive pathway-specific regulator for salinomycin biosynthesis in *Streptomyces albus*. *Applied Microbiology and Biotechnology*, 101, 1547–1557.

SUPPORTING INFORMATION

Additional supporting information can be found online in the Supporting Information section at the end of this article.

How to cite this article: Wei, J., Chen, B., Dong, J., Wang, X., Li, Y. & Liu, Y. et al. (2022) Salinomycin biosynthesis reversely regulates the β-oxidation pathway in *Streptomyces albus* by carrying a 3-hydroxyacyl-CoA dehydrogenase gene in its biosynthetic gene cluster. *Microbial Biotechnology*, 15, 2890–2904. Available from: https://doi.org/10.1111/1751-7915.14145